Periodicity windows in a dynamical system with a delayed feedback

Réal Vallée and Claude Delisle
Laboratoire de Recherche en Optique et Laser (LROL), Département de Physique, Université Laval, Québec, Québec, Canada G1K 7P4
(Received 8 November 1985)

The problem of periodicity windows appearing within the chaotic domain of the hybrid bistable device is considered. New results concerning the frequency-locked waveforms are presented in relation to their stability and their long-lived transients. We also present numerical and experimental results concerning new periodicity windows for a small range of values of the delay ($1<\tau_D<7$). These waveforms appear to be the continuous-time counterparts of the discrete cycles predicted by the one-dimensional model.

I. INTRODUCTION

Among the nonlinear dynamical systems showing transitions between periodic and aperiodic behaviors when a single control parameter is varied, the hybrid bistable device is particularly interesting because of its experimental simplicity and good agreement with the numerical solution of the differential difference equation (DDE) describing it. Moreover, such a system displays a very rich spectrum of dynamical behaviors including the usual period-doubling sequence and other types of first- and second-order transitions between periodic and chaotic waveforms.

The first experimental observation of bifurcations and chaos in a hybrid bistable device was made by Gibbs,[1] Hopf,[2] and collaborators, following a prediction by Ikeda.[3] The experiment was performed with an electro-optic modulator and for a large value of the delay τ_D (in comparison to the response time τ) so that the period-doubling sequence was well described by a simple difference-equation model. However, they did not observe the periodicity windows predicted by the discrete-map model[4] to appear inside the chaotic domain. Instead of these well-known periodic cycles, Hopf *et al.*[2] discovered what they called frequency-locked oscillations. These frequency-locked waveforms were also observed in an acousto-optic bistable device[5] but no observation of periodic cycles arising from the discrete mapping inside the chaotic region has been reported up to now, neither in the electro-optic nor in any other hybrid bistable devices.

This paper concerns these two different types of periodicity windows appearing within the chaotic domain for the hybrid bistable device. New numerical results about the frequency-locked (FL) waveforms will first be brought. Indeed, in a previous numerical analysis[6] the existence of domains of several harmonic solutions in the parameter plane (μ,τ_D) was shown. However, it was not clear from that analysis if the stable FL waveforms observed experimentally were also numerically stable (without any chaotic component). In this paper we show that the FL waveforms are numerically stable for some specific regions in the plane (μ,τ_D). We also report the observation of the periodic cycles within the chaotic domain which have not been observed before. These cycles which are the continuous-time counterpart of the discrete-time periodic cycles arising from the one-dimensional mapping were found for a narrow range of values of the time delay τ_D.

Throughout this paper our description and interpretation of the various waveforms is based on the linearized model recently applied to the hybrid bistable device by Gao *et al.*[7] The reader is therefore referred to Refs. 7 and 8 for more details about this approach. Also the experimental and numerical results are presented in parallel in order to stress the very good agreement between them. The paper is organized as follows. Section II will be devoted to a brief description of the experimental device and of numerical analysis details. In Sec. III the problem of the FL waveforms will be treated. Section IV concerns the description and analysis of new cycles of multiple periods occurring within the chaotic domain.

II. EXPERIMENT AND NUMERICAL ANALYSIS

A detailed description of our device using an acousto-optic modulator as nonlinear element can be found in Ref. 5. In the present experiment an external delay was added in the feedback loop using coaxial cable and/or optical fiber of different lengths. Particular attention was paid to the intrinsic noise level of the device in order to reduce it to its minimum value. Indeed, noise appears to be one of the main causes of the nonobservation of small periodicity windows within the chaotic domain in the previous experiments.

The time evolution of the output of the acousto-optic bistable device is well described by the following DDE:

$$\tau\dot{X}(t)+X(t)=\pi\{A-\mu\sin^2[X(t-\tau_D)-X_B]\}\ . \qquad (1)$$

This equation can only be solved numerically and a Runge-Kutta algorithm of second-order is particularly suitable for that. We solved Eq. (1) keeping the parameters A and X_B fixed at 0.35 and 0.567, respectively, in order to fit the experimental values. The two remaining parameters μ and τ_D therefore define the parameter plane over which steady-state solutions of (1) were searched for. In order to get rid of the long-lived transients we discard-

ed the first 25 000 computation steps of length τ_D where it was necessary. The number N of calculated points or sample for each of these computation steps of length τ_D was fixed to 501. However, in most cases $N=201$ would have been adequate to get a proper simulation of (1).

In order to get a clear and efficient test for distinguishing between chaotic and periodic waveforms, the first Lyapunov exponent (λ_1) was calculated from successive intervals of the trajectories, a positive exponent standing for a chaotic waveform and a zero exponent for a periodic one. As a matter of fact, it was slightly negative for periodic waveforms since it converges to zero from negative values. More details about the computation of the spectrum of Lyapunov exponents for differential-difference equations can be found in Ref. 9.

III. FREQUENCY-LOCKED WAVEFORMS

Derstine and collaborators[10] gave an exhaustive description of the different transitions occurring between stable and unstable FL waveforms. However, it was pointed out by them that the stability properties of these FL waveforms appeared to be complex. Therefore our first concern was to get, if possible, similar experimental results from a different device and to compare these results with the numerical solution of the DDE describing the system. This point is of particular interest since it was stressed by Derstine *et al.* that spurious nonlinearities in the device could greatly perturbate the stability properties of the FL waveforms and that this could explain the poor agreement between their experimental results and a previous numerical analysis. Therefore, it is important to know if the alternate path behavior completely arises from the simple DDE or if one necessarily needs to modify it in order to take into account the small defects of the physical device.

Since we have shown recently[8] that some of the previously called FL waveforms can be simply interpreted as bifurcated structures of higher modes of the system, we will adopt a notation slightly different from that introduced by Derstine *et al.* The letters P, C, and L will still stand for periodic, chaotic, and locked waveforms. The letters P and C will be preceded by a superscript denoting the mode (except for the first mode for which it is implicitly meant) and followed by an integer denoting the bifurcated waveform associated with this mode. For example ^{2}P4 is the period-4 waveform of the second mode. The letter L will be preceded by both a superscript and a subscript denoting the modes between which a locking occurs and followed by an integer denoting the fundamental period of the waveform in $(\tau_D+\tau)$ unit. For example the symbol $^2_1$L4 represents the waveform arising from a locking between the first two modes and having a fundamental period of $4(\tau_D+\tau)$.

A. Crescents of periodicity

Figure 1 shows three sites where the FL waveforms can be found within the chaotic domain. This diagram was obtained by solving Eq. (1) using the procedure described in Sec. II. The parameter plane was systematically covered by increasing τ_D from 2 to 36 by steps of 0.2 for

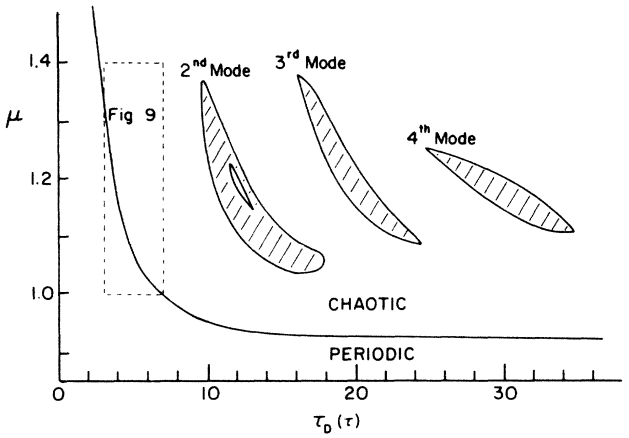

FIG. 1. Location of frequency-locked waveforms in the parameter plane within the chaotic domain.

21 values of μ between 0.9 and 1.4, and μ from 0.9 to 1.4 by steps of 0.005 for 18 values of τ_D between 2 and 36. For each pair of values (μ,τ_D) considered, Eq. (1) was solved, starting from an initial time interval $[0,\tau_D]$ simulating the closure of a switch in the feedback loop. In order to reduce the overall computation time we restricted our analysis to the interval $(0<\tau_D<36)$ so that only the first three crescents where the FL waveforms can be found appear on Fig. 1.

Each of these regions is associated with a mode as one can realize by looking at the fast-oscillation-frequency component of these waveforms. Figure 2(a) shows some of the various stable waveforms found numerically within the first crescent of periodicity $(8<\tau_D<18)$. Some of these waveforms were also observed experimentally [Fig. 3(a)] and it is important to note that their common fast oscillation component has the frequency of the second mode of the system. The waveforms observed within this second-mode crescent are therefore either bifurcated waveforms of the second mode (^{2}P4 being an example of this case) or frequency-locked signals calling in this mode (the $^2_1$L4 waveform, for example). Remarkedly, the two most often seen waveforms of this first crescent, the ^{2}P4 and the $^2_1$L4 waveforms, were also shown to be very stable in the electro-optic experiment for the same range of values of the time delay even if the transmission function of this device is slightly different from our own (acousto-optic). That region of periodic oscillations therefore appears to be typical of a particular range for the delay values. This means that for different values of A or X_B in Eq. (1) or even for a somewhat different transmission function, the FL region would practically just be shifted along the μ axis.

The mechanism underlying the transition between a frequency-locked trajectory and a chaotic one appears to be very sensitive to the external perturbation including those introduced by the numerical analysis. Nevertheless the numerical analysis shows very clearly that these transitions are characterized by hysteresis zone within which a truly periodic and a chaotic attractor coexist. This behavior was also observed experimentally by obtaining

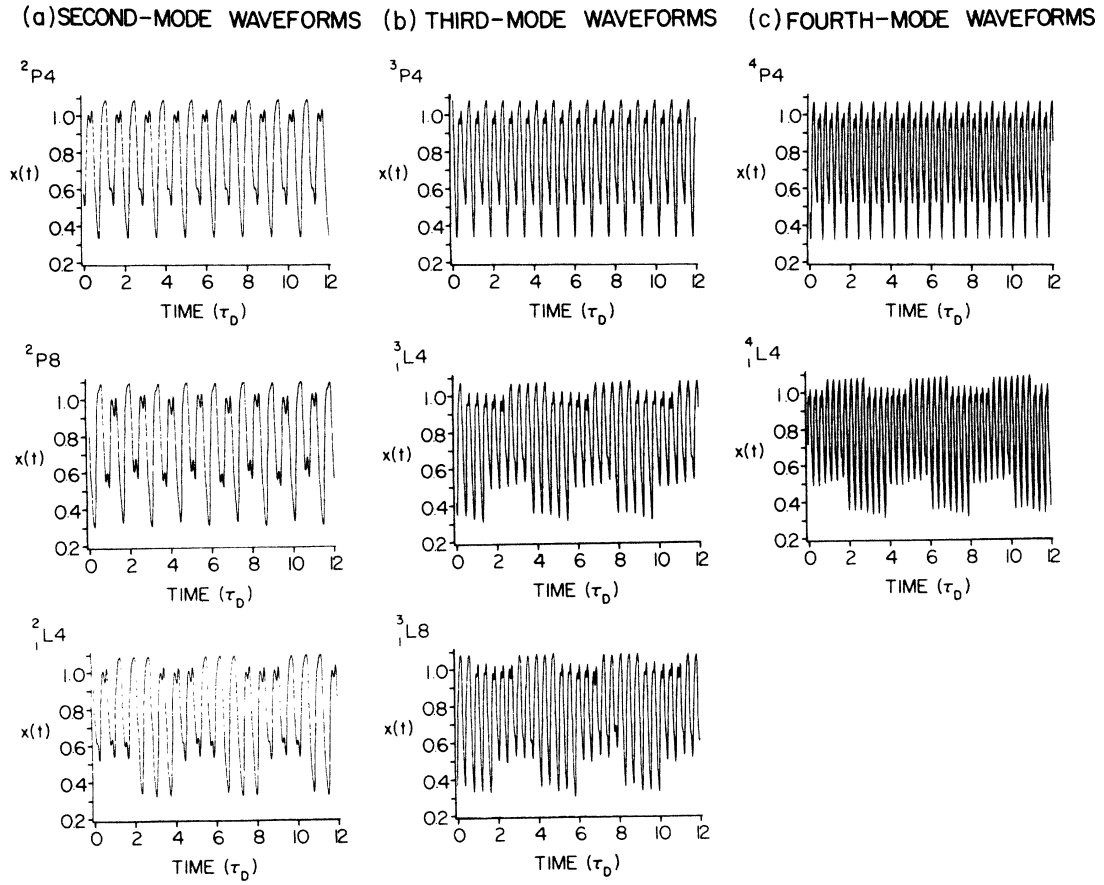

FIG. 2. Numerical frequency-locked waveforms corresponding to the second, third, and fourth linear modes.

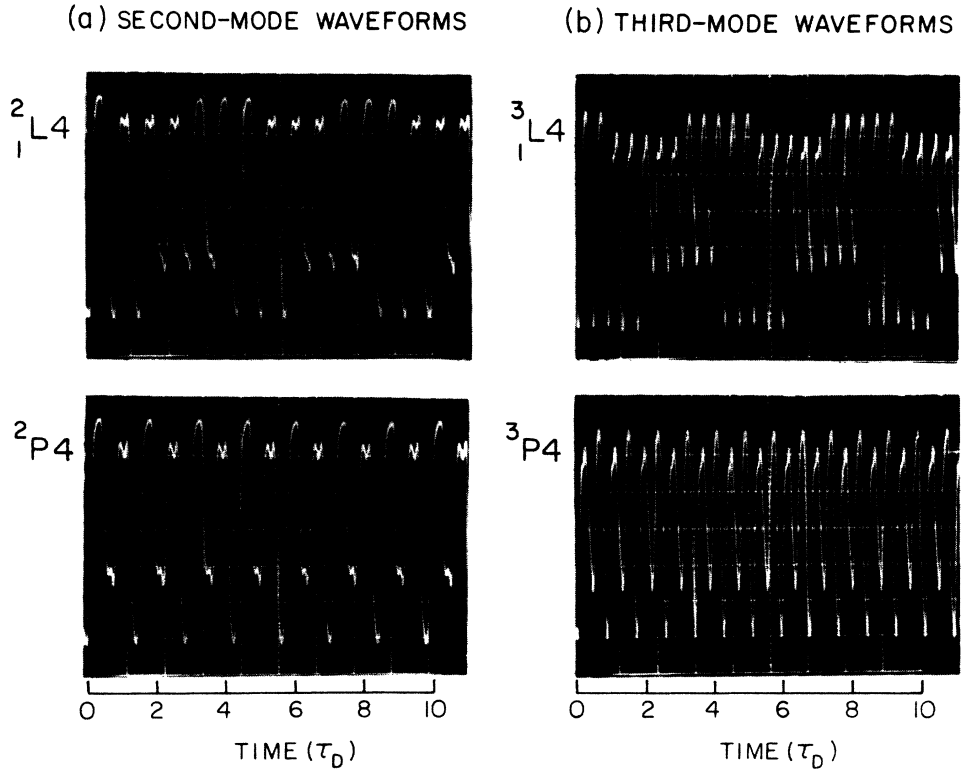

FIG. 3. Experimental frequency-locked waveforms obtained for $\tau_D \simeq 15$. The second-mode waveforms $^2_1$L4 and ^{2}P4 were observed for $\mu = 1.04$ and 1.05, respectively. The third-mode waveforms $^3_1$L4 and ^{3}P4 were observed for $\mu = 1.35$ and 1.29, respectively.

forward (increasing μ) and backward (decreasing μ) bifurcation diagrams for $\tau_D = 15$ (Fig. 4). It is clear from these results that significant differences occur when one decreases instead of increasing μ. (It should be stressed that the frequency of the sweeping signal was low enough so that the output of the system was following μ adiabatically.) The transition from a chaotic to a periodic orbit is characterized by a hysteresis ($0.94 < \mu < 1.05$) such that, by comparison to a usual bistable system, the chaotic orbit corresponds to the lower branch. Indeed, if one reaches the hysteresis zone by decreasing μ and then interrupts temporarily the feedback loop (cutting the laser ray), the frequency-locked waveform is destroyed and a chaotic one sets in and reappears after any further interruption.

When μ is increased beyond 1.05 the periodic waveforms then become the only steady-state orbits substained by the system. This window of periodicity comes to an end near $\mu = 1.10$ where the chaos reappears. But on the contrary to the transition from chaos to periodicity this transition from periodicity to chaos is not accompanied by a hysteresis and it occurs in an abrupt manner resembling an interior crisis.[11] This sequence of phenomena is summarized in the diagram of Fig. 5. Let us first mention about this diagram that it depicts a scenario observed experimentally but which is in very good agreement with the numerical results. It should also be stressed that this diagram corresponds to a typical but not exclusive type of behavior for a system described by an equation such as Eq. (1). However, the main features of this scenario are very interesting because they describe a particular mechanism by which a dynamical system can become more chaotic as the nonlinearity is increased. Moreover, the whole sequence can be regarded as a competition mechanism between the first and the second mode leading the system to undergo a transition from a $^1C2$ to a $^2C2$ chaotic oscillation.

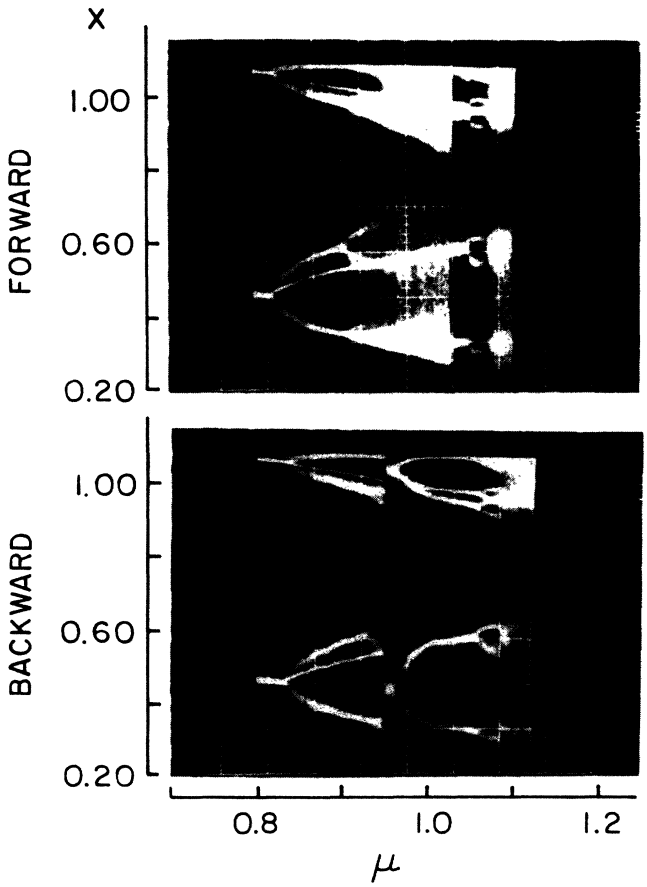

FIG. 4. Experimental forward (increasing μ) and backward (decreasing μ) bifurcation diagrams for $\tau_D \simeq 15$. The full range sweeping time was 100 sec.

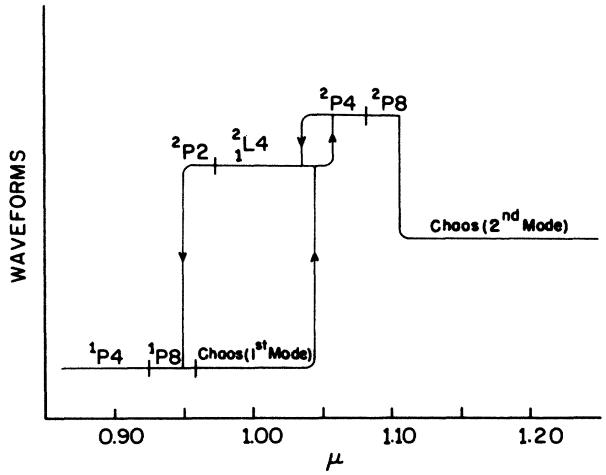

FIG. 5. Diagram of the transitions occurring between waveforms found inside the first crescent. This scheme is based on experimental results obtained for $\tau_D \simeq 15$.

There appears on Fig. 1 a second group of periodic waveforms within the crescent located inside the interval $16 < \tau_D < 24$. All the waveforms of this group have a fast oscillation corresponding to the third mode of the system. Some of them are shown in Fig. 2(b). Moreover, the hysteresis occurring at the lower boundary of the second-mode region also occurs at the boundary of the third-mode region. Finally, a third crescent of periodicity can be observed on Fig. 1 for $24 < \tau_D < 34$ and the periodic waveforms inside this region correspond as expected to the fourth mode of the system [Fig. 2(c)].

B. The frequency-locked time transients

An interesting phenomenon is observed when one considers the number of time intervals $[t - \tau_D, t]$ that one has to compute before getting a steady-state FL waveform. As a matter of fact within the first crescent the time transient necessary for the system to reach a given periodic waveform was almost always smaller than $2000\tau_D$. For the second crescent one has sometimes to compute more than 15 000 time intervals in order to reach a periodic orbit and the situation was even worse for the third crescent associated with the fourth mode. Furthermore, we checked that once the system has reached one of the periodic attractors it remains locked to its afterwards. This phenomenon is particularly interesting if we consider that the rate of exponential divergence of the trajectories

is such that all the information about the initial conditions is completely lost after less than $200\tau_D$. So it was even more surprising to note that this unusual time transient was, however, dependent on the initial conditions. A convenient way to understand this peculiar transient is to follow the temporal evolution of a trajectory starting from a given initial condition. To do this we calculated the first Lyapunov exponent λ_1 over successive intervals ($100\tau_D$ long) of the trajectory. Figure 6 shows the results of this analysis for $\tau_D=21.73$ and $\mu=1.138$. One can see that the trajectory rapidly reaches a "chaotic state" characterized by a positive λ_1 approximately equal to 0.009 (in τ^{-1} unit). The λ_1 oscillates around this value for about $6000\tau_D$ until an abrupt jump occurs and a periodic trajectory sets in. Therefore a first interesting point to note is that this transition from chaoticity to periodicity is not a smooth one spread over the first $6000\tau_D$ but a very abrupt one. Moreover, we can estimate by looking directly at the temporal signal in the transition region that the real transient was about $150\tau_D$ long. A second very interesting point is that if we compute the trajectory keeping exactly the same values for μ and τ_D but starting from a different initial condition for $X(t)$ over the first time interval $[0,\tau_D]$, the abrupt jump occurs at a completely different and unpredictable time. In other words this jump can occur after $500\tau_D$ as well as after $10\,000\tau_D$ depending on our choice of the initial condition.

To illustrate this behavior we performed a simple experiment resembling that introduced by Shaw for a 1-D map.[12] We first computed the trajectories corresponding to 600 different initial conditions keeping μ and τ_D constant. We then calculated the number of trajectories (the survivors) which were still chaotic after a given time. The logarithm of the number of these "survivors" is plotted as a function of time on Fig. 7. We clearly note an exponential decrease of the number of survivors as a function of time and this behavior may be interpreted as a probability for the system to become periodic when it lies on a kind

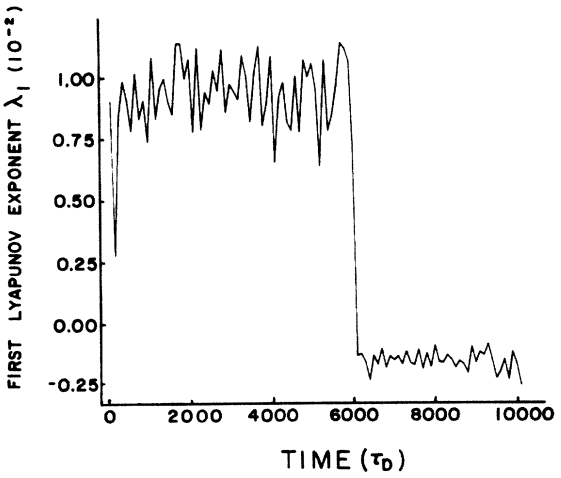

FIG. 6. Graph of the first Lyapunov exponent as a function of time. Each point of this plot corresponds to the value of λ_1 computed over time intervals ($100\tau_D$ long) of the trajectory for $\tau_D=21.73$ and $\mu=1.138$.

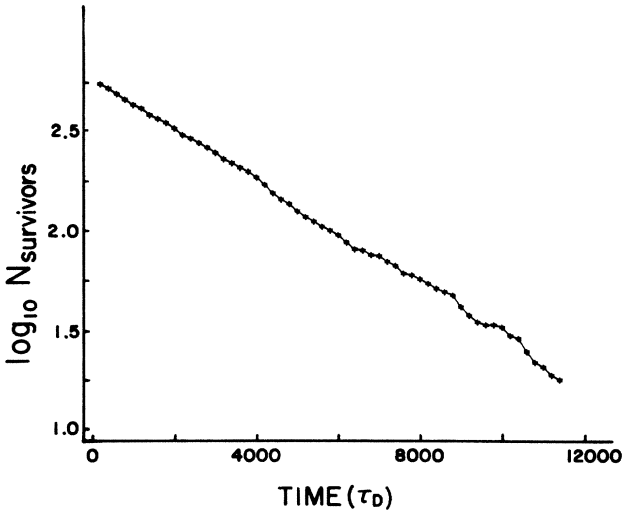

FIG. 7. Logarithm of the number of remaining chaotic trajectories (survivors) as a function of time for $\tau_D=21.73$ and $\mu=1.138$.

of "metastable" chaotic orbit. As a matter of fact it is not so surprising that the time necessary for the system to reach a periodic state depends on the initial conditions even if these initial conditions are lost after less than a few hundred τ_D. Indeed two different initial conditions rapidly become indistinguishable after a certain time and the two subsequent trajectories obviously remain different. Now these trajectories will both visit every point of the same chaotic attractor but at different moments. Therefore if the basin of attraction of the periodic attractor is viewed as a "target" which can be reached with a given probability by the chaotic trajectory it is easy to understand that the event "hitting the target" can occur at very different times depending specifically on the trajectory which is considered. In other words one can say that the neighboring basin of attraction of these FL waveforms is very localized in the phase space but this basin is somehow connected to a surrounding chaotic set.

Since the first submission of this paper we came upon a publication by Kantz and Grassberger[13] discussing thoroughly the problem of long-lived transients in various systems. It appears that the particularly long transients we observed in the computation of frequency-locked waveforms illustrate very well this phenomenon.

IV. PERIODIC CYCLES

A. Disappearing P3 cycle

The DDE modeling systems with delayed feedback like the acousto-optic device displays various dynamical behavior depending on the ratio between the time delay and the response time of the system. In the case where $\tau_D \gg \tau$, one may expect that the difference equation (DE) obtained by neglecting the differential term of (1) would provide a good discrete-time approximation of the continuous-time DDE. However, this approximation appears to be correct only for describing the period-doubling

sequence following the first threshold of instability and in the limit of large delay. As a matter of fact the DDE and its associated DE display completely different behaviors within the chaotic region. Heuristically speaking, one can say that these systems with delayed feedback behave as if they were driven by two opposite tendencies, one coming from the time retardation which induces a discontinuous discrete mapping behavior and the other coming from the time response of the physical device which fix some constraints on the fast temporal changes.

This dual behavior clearly appears when one looks at the transient state of the system immediately after it has been switched on. This was done experimentally by introducing an electronic switch in the feedback loop. The switch was triggered on and off by an external function generator while the parameter μ was slowly varied until an unstable periodicity window was reached. For a sufficiently large value of the delay (typically $\tau_D > 20$) one can see a progressive deterioration of the corresponding waveform. Figure 8(a) shows such a deterioration for the waveform corresponding to the P3 cycle. One clearly distinguishes at first a periodic oscillation of period $3(\tau_D + \tau)$. However, the "plateaux" of this waveform are gradually shortened from one iteration to the next by a growing fast oscillation which finally destroys the discrete behavior. Such a phenomenon was also obtained numerically [Fig. 8(b)] and we could derive that in the limit of large delay the destruction time was directly given by $\tau_D^2/2$ (τ being the time unit). In other words each "plateau" of length τ_D is shortened by an amount of 2 (fast oscillation cycle) at each iteration of the map. This very interesting phenomenon provides an experimental demonstration of the fact that the differential term cannot be simply eliminated from (1) in the limit of large delay. Indeed the longer the delay is, the longer will be the transient necessary to eliminate the discrete mapping structure but this structure will always be destroyed eventually. A simple interpretation of these results is provided by the linear model which predicts that more higher modes become unstable for larger values of the time delay so that a given periodic cycle associated with the first mode—which would be sustained by the system if this mode was alone—is rapidly destroyed by the fast oscillations arising from the unstable higher modes. Obviously this picture is heuristic since the linear model can only predict the thresholds of instability of the modes and not the boundedness of the trajectories which arises from the nonlinearity. However, according to this linearized approach it would be possible to observe these periodic cycles corresponding to the discrete mapping in the intermediate zone where τ_D is still larger than τ but small enough so that the first mode is the only unstable one.

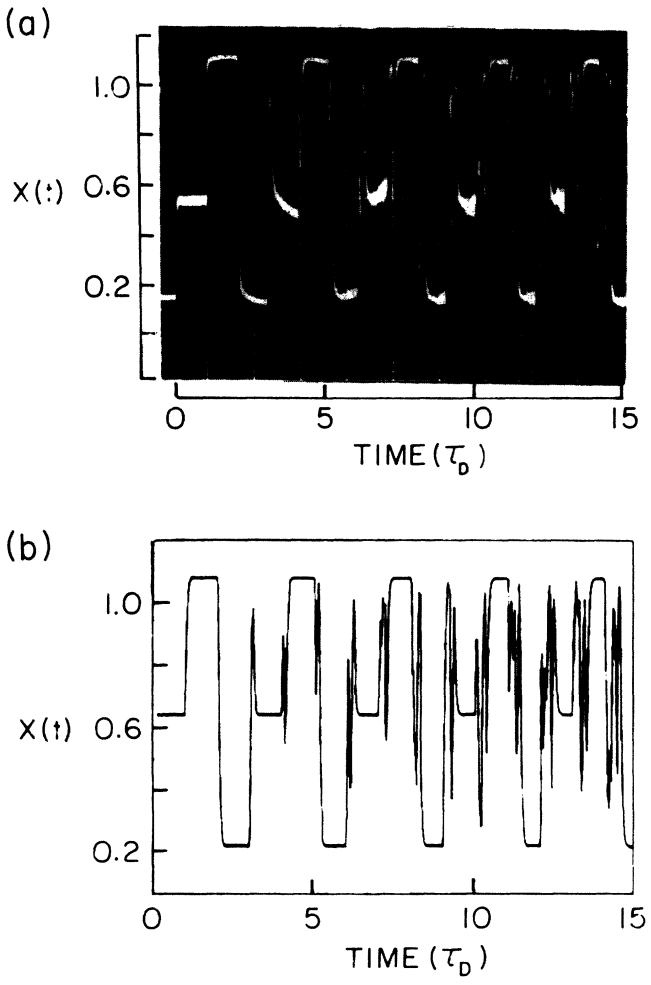

FIG. 8. Progressive destruction of the unstable P3 cycle for $\tau_D \simeq 40$ and $\mu = 1.13$ for the experimental signal in (a) and $\mu = 1.18$ for the numerical one in (b).

B. Even periodic cycles

In order to verify this we performed a large scale analysis of the small area of the parameter plane defined

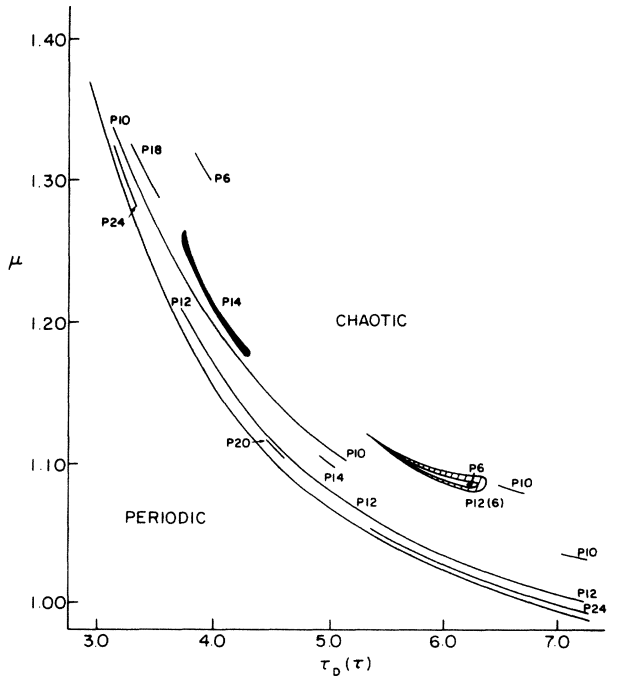

FIG. 9. Location of the even periodic waveforms in the parameter plane.

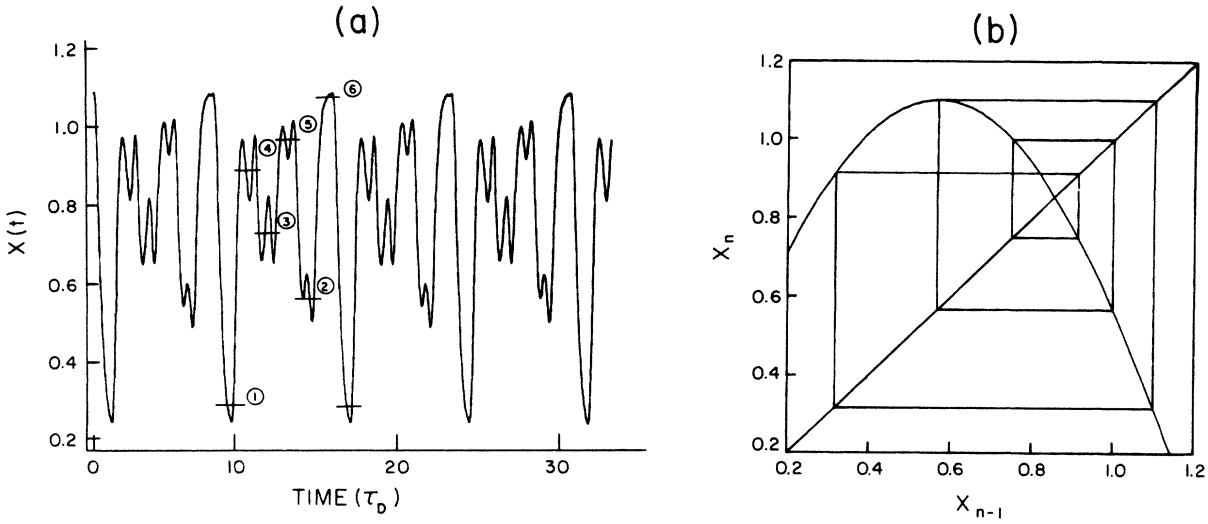

FIG. 10. (a) Numerical P6 waveform for $\tau_D = 6.25$ and $\mu = 1.085$. (b) Discrete P6 cycle of the difference equation corresponding to Eq. (1), for $\mu = 0.9667$.

by $3 < \tau_D < 7$ and $1.0 < \mu < 1.4$. Figure 9 shows the results of this numerical analysis. Remarkedly, a rich variety of periodic waveforms were found within this region. Most of the even periodic cycles up to P24 are present and we note that their corresponding windows are systematically parallel to the accumulation line separating the periodic and chaotic domains. Figure 10(a) shows a typical computed waveform (the P6 waveform). Aside from the fact that the period of this oscillation is $6(\tau_D + \tau)$ it is easy to convince oneself that this is indeed a continuous-time version of the P6 discrete cycle by considering the closed loop in the discrete map corresponding to this cycle [Fig. 10(b)]. By numbering the six levels from the lower to the upper one we get the sequence (1-4-3-5-2-6-1) which corresponds to the sequence of the continuous waveform. We will use thereafter this characteristic sequence to identify the various periodic cycles. This will be especially useful for distinguishing the different isomeric forms having the same period. Moreover, this sequence is more convenient for identifying a temporal signal than the usual "right" (R) and "left" (L) characteristic sequence.[14] Nevertheless we will indicate by an asterisk the level corresponding to the "center" (C) of the equivalent map so that the correspondence between the two characteristic sequences will be easy to establish. For instance in the sequence (1-4-3-5-2*-6-1) the level two corresponds to C of the map. Therefore an upper level is said to be right and a lower one to be left so that we get the sequence (RLR^3).

Figure 11 shows the even periodic computed waveforms (up to P14) and their characteristic sequences. The particular shape of these waveforms can be regarded as resulting from a phase-locking between a long periodic structure prescribed by the discrete mapping and a fast oscillation component which correspond to the second mode. This can be understood by remembering first that all over the region where these cycles were found the first linear eigenmode is the only unstable one (its eigenvalue real part α_1 being positive). Remembering also that the real part of the second-mode eigenvalue is nearly zero ($\alpha_2 < 0$) and finally that the other mode real parts are negligible, the system can therefore be described as a two-mode problem where the second mode is slaved by the first one. Obviously this is a very peculiar situation since it occurs only for a small range of values of the time delay.

TABLE I. Characteristic sequences of the periodic cycles for the discrete model.

Superstable orbit	Cycle	Characteristic Sequence
0.9066	P8(4)	(1-5-4-7-2-6-3*-8-1)
0.9292	P12	(1-7-6-10-3-9-4-11-2-8-5*-12-1)
0.9416	P14	(1-8-7-11-4-12-3-10-5-13-2-9-6*-14-1)
0.9484	P10	(1-6-5-8-3-9-2-7-4*-10-1)
0.9551	P14	(1-8-7-11-4-13-2-9-6-12-3-10-5*-14-1)
0.9667	P6	(1-4-3-5-2*-6-1)
0.9697	P12(6)	(1-7-6-9-4-11-2-8-5-10-3*-12-1)
0.9827	P10	(1-6-5-7-4-9-2-8-3*-10-1)
0.9894	P12	(1-7-6-8-5-10-3-11-2-9-4*-12-1)
0.9951	P8	(1-5-4-6-3-7-2*-8-1)
1.0039	P10	(1-6-5-7-4-8-3-9-2*-10-1)

We observed experimentally many of these periodic cycles and found their shapes to be identical to the computed ones. Figure 12 shows some of these experimental waveforms as well as their characteristic sequences. In the case of the P10, P12, and P14 waveforms it is important to note that the intrinsic noise level of the device was just slightly under the threshold value for which the detection is possible. On the other hand, Fig. 9 shows waveforms of longer periods (up to P24) obtained from the numerical analysis. Moreover, we verified that it was possible to get waveforms with longer periods by increasing the computation resolution. Therefore there seems to be no theoretical limitation to the observation of all the even periodic cycles predicted by the discrete model. The real limitation is "noise," understood in a large sense.

Let us add a few words about the order of appearance of these waveforms as μ is increased. To do so we draw a parallel between the order of occurrence in both the continuous and the discrete cases. The order of occurrence for the even discrete cycles (up to P14) is shown in Table I and corresponds as expected to the U sequence.[14] A similar sequence is obtained for the even continuous waveforms if one considers, instead of μ only, the geometrical distance in the parameter plane separating a given window from the accumulation line. Indeed, if one orders the waveforms, according to their separation from the accumulation line, one can see that the U sequence appears to be valid for the continuous periodic waveforms too (Fig. 9).

C. Odd periodic cycles

No odd periodic cycles were found within the area of the parameter plane shown on Fig. 9. A simple explanation for this can be stated as follows. We have shown that there must exist a frequency locking between the first two modes for these cycles to be sustained by the system. Now it is easy to understand that this frequency locking cannot occur for an odd periodic waveform in a region

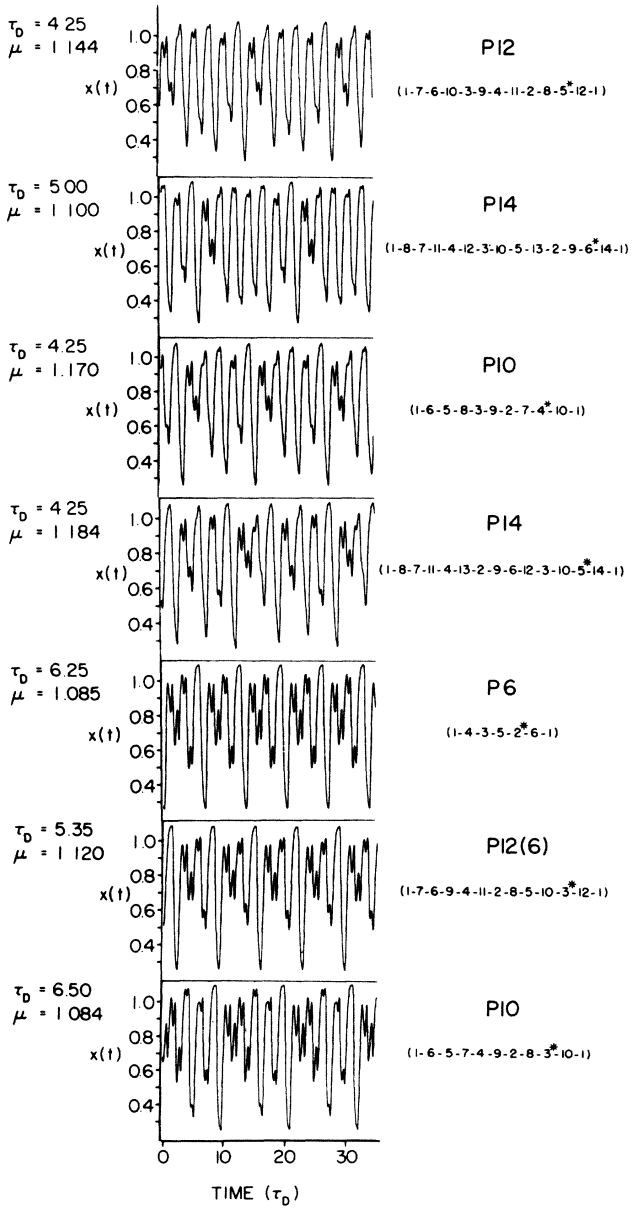

FIG. 11. Numerical even periodic waveforms. The P12(6) waveform arises from a period doubling of the preceding P6 waveform.

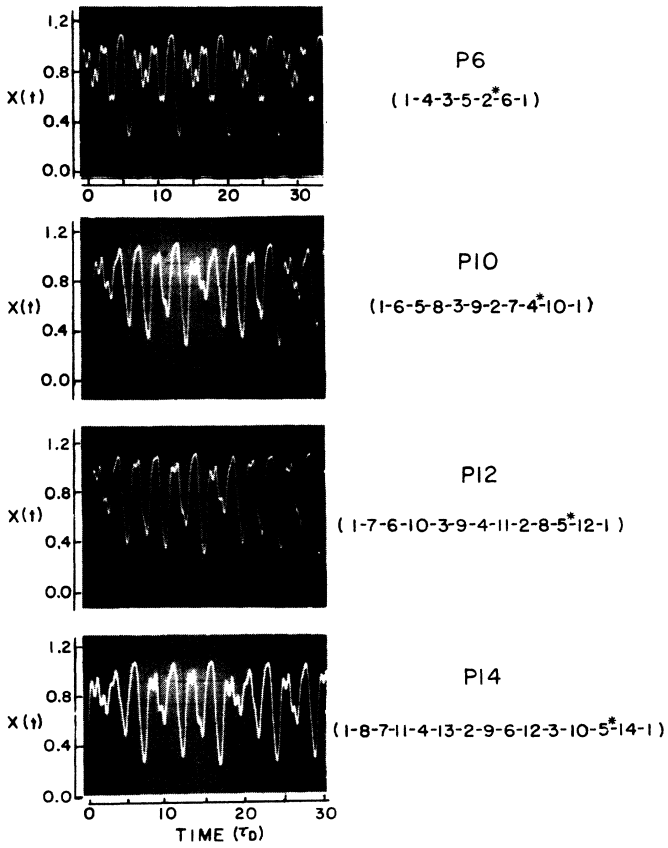

FIG. 12. Experimental even periodic waveforms. The P6 waveform was obtained for $\tau_D \simeq 4.2$ and $\mu = 1.17$. The P12, P10, and P14 waveforms were obtained for $\tau_D \simeq 3.5$ and $\mu = 1.26$, 1.29, and 1.31, respectively.

where the frequency corresponding to the second mode is three times that of the first mode (which is the condition for the even cycles to be sustained). For instance, a P6 cycle corresponds exactly to nine oscillation cycles of the second mode, but a P5 cycle would have to correspond to 7.5 cycles of this mode. Fortunately a circumstance greatly enhances the possibility of getting a ratio between the periods of oscillation of the first two modes different from three. Indeed, according to the linear model this ratio is significantly larger than three for small value of τ_D. Also Fig. 9 shows that the whole sequence of phenomena appears to be stretched and shifted along the μ axis as the delay is decreased.

Consequently many odd periodic waveforms were observed, but for small values of τ_D and for significantly larger values of μ. Figure 13 shows the odd periodic waveforms that we could observe experimentally and Fig. 14 some of the computed ones with their characteristic sequences. Incidentally the shape of these waveforms is such that it is not so obvious that they are continuous-time counterparts of discrete periodic cycles. However, if one examines, for instance, the P5 waveforms shown on Fig. 13 one can see that their characteristic sequences as well as their fundamental periods correspond to those of P5 discrete cycles. The main difference between an odd and an even periodic waveform is that the odd one cannot simply oscillate "up" and "down" over its entire cycle. There must be an up-up-down sequence for a part of its cycle and this sequence seems to amplify the fast oscillation component of the waveform. Nevertheless the interpretation of the various periodic waveforms in terms of a discrete-mapping process becomes very troublesome for values of τ_D around two and practically illusive for $\tau_D < 2$. As a matter of fact we have found other periodic cycles within the interval $1 < \tau_D < 2$ which can hardly be associated with any discrete cycle but this is not really surprising since the response time is now almost equal to the retardation time. On the contrary, what is more surprising is that a discrete-mapping process had kept on prevailing for such small values of the delay.

V. CONCLUSION

In addition to the previously found frequency-locked waveforms which arise from a continuous-time process, the hybrid bistable device can also display continuous-

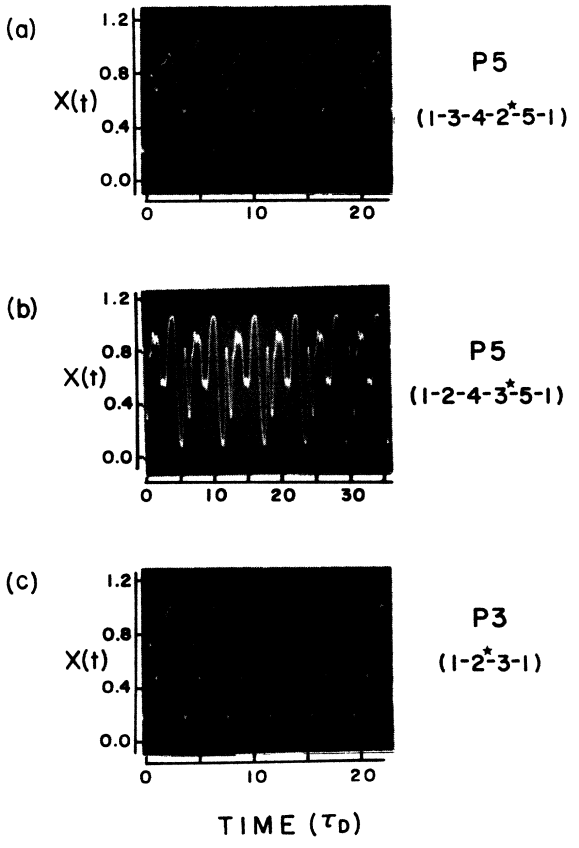

FIG. 13. Experimental odd periodic waveforms obtained: (a) for $\tau_D \simeq 1.8$ and $\mu = 1.80$; (b) for $\tau_D \simeq 4.2$ and $\mu = 1.47$; (c) for $\tau_D \simeq 1.8$ and $\mu = 2.11$.

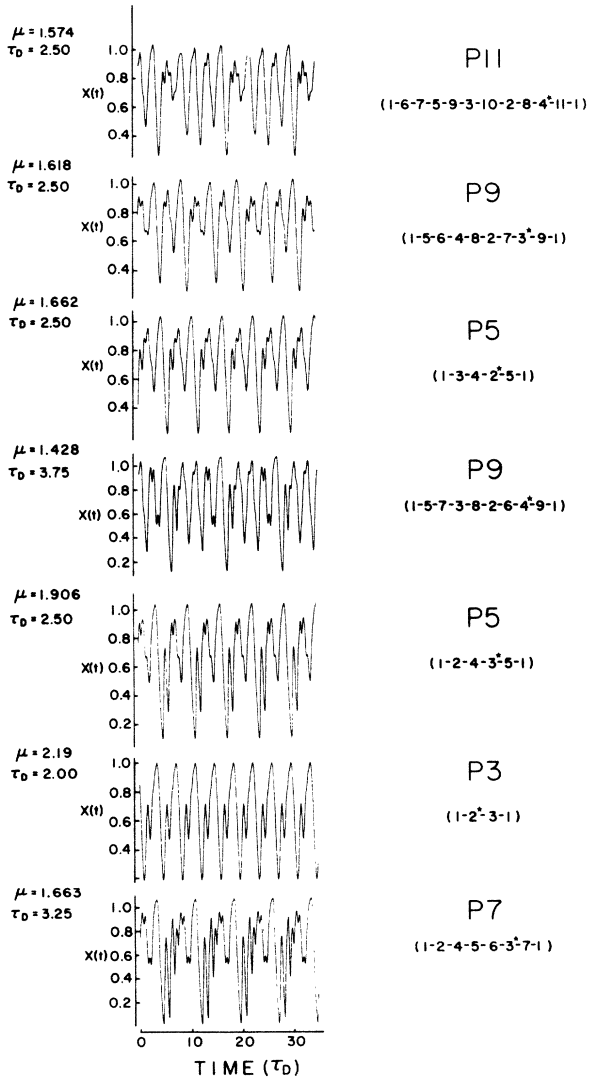

FIG. 14. Numerical odd periodic waveforms.

time counterparts of the periodic cycles of the DE associated to the DDE describing the system. These two types of periodic waveforms are found within separated regions of the parameter plane and can be interpreted in terms of modes of the system. Concerning the frequency-locked waveforms, we have shown that, within the region covered by our analysis ($\tau_D < 36$), they always arise from a locking between only two modes and that the first mode is always one of these two modes. Also the stable numerical FL waveforms are localized within crescentlike regions of the parameter plane characterized by a certain range of values of the delay. Moreover, a particularly long transient state encountered before reaching a FL orbit was shown to be typical of these periodic waveforms. This transient can be simply interpreted as a metastable chaotic orbit and this interpretation is convenient for describing the transition between a chaotic and a FL orbit. We have also obtained both numerically and experimentally the continuous-time versions of the periodic cycles of the DE associated with Eq. (1). These waveforms are sustained by the system for small values of the delay and a two-mode interaction can be considered to describe them, where the second mode is slaved by the first one. We observed both odd and even periodic cycles but they appeared within distinct regions of the parameter plane.

We have shown how the periodic waveforms encountered in this analysis can be interpreted in term of modes of the system. Particularly the number of modes participating in the dynamics of the system increases with the delay and this is reflected in the parameter plane by the appearance of different periodicity regions associated with different modes. In this manner the linear model is convenient for describing the various periodic waveforms. However, one must remember that this model can only predict solutions (linear modes) which go to infinity as their thresholds of stability are crossed. In other words the linear model does not explain the boundedness of the trajectories which arises from the nonlinearity. However, the experimental results clearly show that the dynamical evolution of the system is governed by the interaction between real underlying modes. Therefore it appears that a better description of the hybrid bistable device on a theoretical basis would have to include the nonlinear interactions between the modes, from which the main features of the system arise.

ACKNOWLEDGMENTS

One of us (R.V.) would like to thank M. W. Derstine and F. A. Hopf. This work was supported by the Natural Sciences and Engineering Research Council of Canada.

[1]H. M. Gibbs, F. A. Hopf, D. L. Kaplan, and R. L. Shoemaker, Phys. Rev. Lett. **46**, 474 (1981).

[2]F. A. Hopf, D. L. Kaplan, H. M. Gibbs, and R. L. Shoemaker, Phys. Rev. A **25**, 2172 (1982).

[3]K. Ikeda, Opt. Commun. **30**, 257 (1979).

[4]See, for example, R. M. May, Nature **261**, 459 (1976).

[5]J. Chrostowski, R. Vallée, and C. Delisle, Can. J. Phys. **61**, 1143 (1983).

[6]K. Ideka, K. Kondo, and O. Akimoto, Phys. Rev. Lett. **49**, 1467 (1982).

[7]J. Y. Gao, L. M. Narducci, L. S. Shulman, M. Squicciarini, and J. M. Yuan, Phys. Rev. A **28**, 2910 (1983).

[8]R. Vallée, and C. Delisle, IEEE J. Quantum Electron. **QE21**, 1423 (1985).

[9]G. Benettin, L. Galgani, A. Giorgilli, and J. M. Strelcyn, Mecanica **15**, 9 (1980).

[10]M. W. Derstine, H. M. Gibbs, F. A. Hopf, and D. L. Kaplan, Phys. Rev. A **27**, 3200 (1983).

[11]C. Gregobi, E. Ott, and J. A. Yorke, Phys. Rev. Lett. **22**, 1507 (1982).

[12]R. Shaw, Z. Naturforsch **36a**, 80 (1981).

[13]H. Kantz and P. Grassberger, Physica **17D**, 75 (1985).

[14]N. Metropolis, M. L. Stein, and P. R. Stein, J. Comb. Theory, Ser. A **15**, 25 (1973).

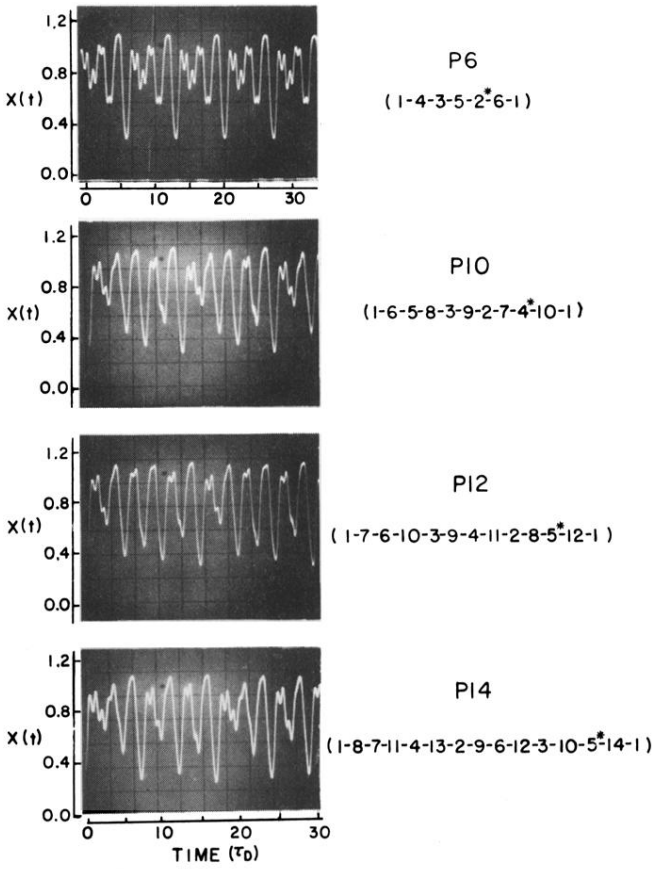

FIG. 12. Experimental even periodic waveforms. The P6 waveform was obtained for $\tau_D \simeq 4.2$ and $\mu = 1.17$. The P12, P10, and P14 waveforms were obtained for $\tau_D \simeq 3.5$ and $\mu = 1.26$, 1.29, and 1.31, respectively.

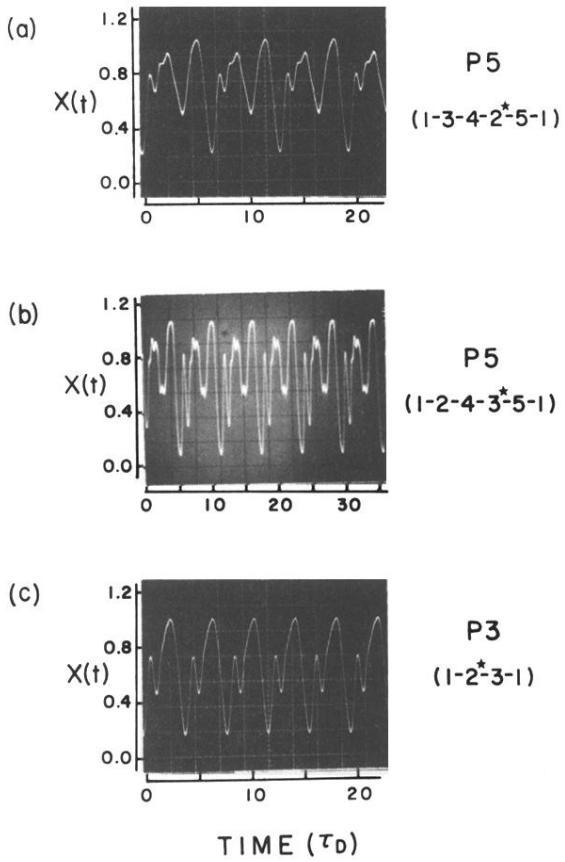

FIG. 13. Experimental odd periodic waveforms obtained: (a) for $\tau_D \simeq 1.8$ and $\mu = 1.80$; (b) for $\tau_D \simeq 4.2$ and $\mu = 1.47$; (c) for $\tau_D \simeq 1.8$ and $\mu = 2.11$.

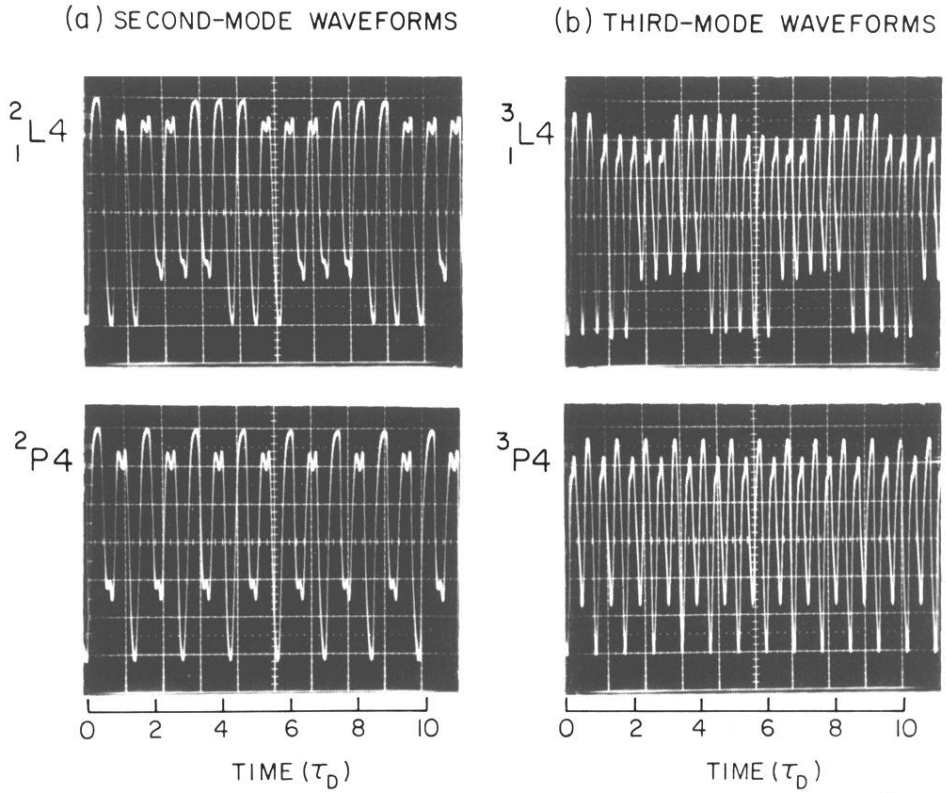

FIG. 3. Experimental frequency-locked waveforms obtained for $\tau_D \simeq 15$. The second-mode waveforms $^{2}_{1}$L4 and ^{2}P4 were observed for $\mu = 1.04$ and 1.05, respectively. The third-mode waveforms $^{3}_{1}$L4 and ^{3}P4 were observed for $\mu = 1.35$ and 1.29, respectively.

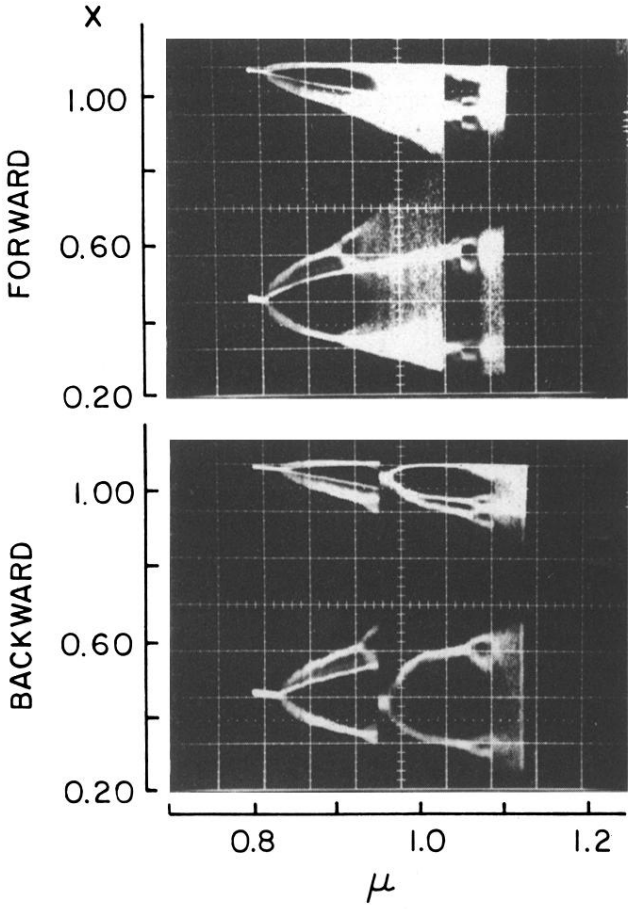

FIG. 4. Experimental forward (increasing μ) and backward (decreasing μ) bifurcation diagrams for $\tau_D \simeq 15$. The full range sweeping time was 100 sec.

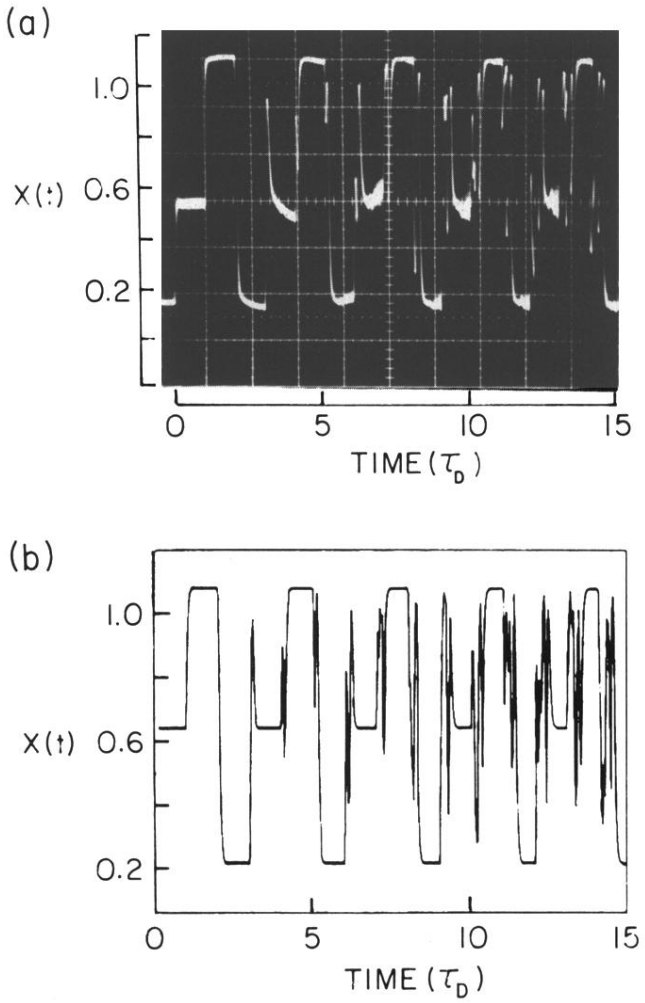

FIG. 8. Progressive destruction of the unstable P3 cycle for $\tau_D \simeq 40$ and $\mu = 1.13$ for the experimental signal in (a) and $\mu = 1.18$ for the numerical one in (b).